as well, for which less topological information is currently available, including such important examples as genetic or signaling networks in biological systems. We often do not think of biological systems as open or growing, because their features are genetically coded. However, possible scale-free features of genetic and signaling networks could reflect the networks' evolutionary history, dominated by growth and aggregation of different constituents, leading from simple molecules to complex organisms. With the fast advances being made in mapping out genetic networks, answers to these questions might not be too far away. Similar mechanisms could explain the origin of the social and economic disparities governing competitive systems, because the scale-free inhomogeneities are the inevitable consequence of self-organization due to the local decisions made by the individual vertices, based on information that is biased toward the more visible (richer) vertices, irrespective of the nature and origin of this visibility.

References and Notes

1. R. Gallagher and T. Appenzeller, *Science* **284**, 79 (1999); R. F. Service, *ibid.*, p. 80.
2. G. Weng, U. S. Bhalla, R. Iyengar, *ibid.*, p. 92.
3. C. Koch and G. Laurent, *ibid.*, p. 96.
4. S. Wasserman and K. Faust, *Social Network Analysis* (Cambridge Univ. Press, Cambridge, 1994).
5. Members of the *Clever* project, *Sci. Am.* **280**, 54 (June 1999).
6. R. Albert, H. Jeong, A.-L. Barabási, *Nature* **401**, 130 (1999); A.-L. Barabási, R. Albert, H. Jeong, *Physica A* **272**, 173 (1999); see also http://www.nd.edu/~networks.
7. P. Erdős and A. Rényi, *Publ. Math. Inst. Hung. Acad. Sci.* **5**, 17 (1960); B. Bollobás, *Random Graphs* (Academic Press, London, 1985).
8. S. Lawrence and C. L. Giles, *Science* **280**, 98 (1998); *Nature* **400**, 107 (1999).
9. In addition to the distribution of incoming links, the WWW displays a number of other scale-free features characterizing the organization of the Web pages within a domain [B. A. Huberman and L. A. Adamic, *Nature* **401**, 131 (1999)], the distribution of searches [B. A. Huberman, P. L. T. Pirolli, J. E. Pitkow, R. J. Lukose, *Science* **280**, 95 (1998)], or the number of links per Web page (*6*).
10. D. J. Watts and S. H. Strogatz, *Nature* **393**, 440 (1998).
11. S. Redner, *Eur. Phys. J. B* **4**, 131 (1998).
12. We also studied the neural network of the worm *Caenorhabditis elegans* (*3, 10*) and the benchmark diagram of a computer chip (see http://vlsicad.cs.ucla.edu/~cheese/ispd98.html). We found that $P(k)$ for both was consistent with power-law tails, despite the fact that for *C. elegans* the relatively small size of the system (306 vertices) severely limits the data quality, whereas for the wiring diagram of the chips, vertices with over 200 edges have been eliminated from the database.
13. S. Milgram, *Psychol. Today* **2**, 60 (1967); M. Kochen, ed., *The Small World* (Ablex, Norwood, NJ, 1989).
14. J. Guare, *Six Degrees of Separation: A Play* (Vintage Books, New York, 1990).
15. M. Barthélémy and L. A. N. Amaral, *Phys. Rev. Lett.* **82**, 15 (1999).
16. For most networks, the connectivity m of the newly added vertices is not constant. However, choosing m randomly will not change the exponent γ (Y. Tu, personal communication).
17. W. B. Arthur, *Science* **284**, 107 (1999).
18. Preferential attachment was also used to model evolving networks (L. A. N. Amaral and M. Barthélémy, personal communication).
19. J. R. Banavar, A. Maritan, A. Rinaldo, *Nature* **399**, 130 (1999).

20. We thank D. J. Watts for providing the *C. elegans* and power grid data, B. C. Tjaden for supplying the actor data, H. Jeong for collecting the data on the WWW, and L. A. N. Amaral for helpful discussions. This work was partially supported by NSF Career Award DMR-9710998.

24 June 1999; accepted 2 September 1999

Osmium Isotope Constraints on Ore Metal Recycling in Subduction Zones

Brent I. A. McInnes,[1]* Jannene S. McBride,[2] Noreen J. Evans,[1] David D. Lambert,[2] Anita S. Andrew[3]

Veined peridotite xenoliths from the mantle beneath the giant Ladolam gold deposit on Lihir Island, Papua New Guinea, are 2 to 800 times more enriched in copper, gold, platinum, and palladium than surrounding depleted arc mantle. Gold ores have osmium isotope compositions similar to those of the underlying subduction-modified mantle peridotite source region, indicating that the primary origin of the metals was the mantle. Because the mantle is relatively depleted in gold, copper, and palladium, tectonic processes that enhance the advective transport and concentration of these fluid soluble metals may be a prerequisite for generating porphyry-epithermal copper-gold deposits.

The tectonic relationship between subduction-related magmatism at convergent margins and porphyry copper-gold (Cu-Au) ore formation has long been recognized (*1*). However, the physical and chemical processes that govern Cu-Au metallogeny and the ultimate source(s) of the metals in these ore deposits are poorly understood. The rhenium-osmium (Re-Os) isotopic system (based on the β^- decay of ^{187}Re to ^{187}Os) is a tracer of metallogenic processes at convergent margins because both elements have geochemical properties similar to metals that occur in porphyry ore deposits (*2, 3*). Because Re is highly concentrated in crustal rocks and Os is concentrated in the mantle (*4, 5*), this isotopic system is particularly useful for quantifying the flux of ore elements in island arc settings where the two principal reservoirs for metals are subducted crust and mantle wedge peridotite.

Os isotope studies in subduction zones are currently limited because of the rarity of deep-seated suprasubduction samples (rocks overlying a subducted slab). Previous studies (*6, 7*) have demonstrated that radiogenic Os is introduced into the subarc mantle by hydrous, oxidizing fluids derived during slab dehydration. We report on results from a suprasubduction xenolith locality, the Tubaf seamount in the Lihir island group of the Tabar-Lihir-Tanga-Feni island arc in Papua New Guinea (Fig. 1). This xenolith locality is important for the following reasons: (i) it contains samples that represent a complete section of oceanic lithosphere at an intraoceanic convergent margin, (ii) it is located adjacent to one of the world's largest and youngest volcano-hosted Au deposits, and (iii) it contains metasomatized mantle peridotite xenoliths with Au-enriched vein minerals that crystallized in the mantle from oxidizing, alkali- and sulfur-rich hydrous fluids.

During the oceanographic investigation of submarine hydrothermal systems in Papua New Guinea (*8*), a submarine cinder cone (Tubaf volcano, 1280 m below sea level; 3° 15.25′ S, 152° 32.50′ E) was discovered 14 km southwest of the giant Ladolam gold mine (>40 million oz contained Au) on Lihir Island. Dredge and video-grab sampling of the 1-km-diameter volcanic cone returned 130 ultramafic, mafic, and sedimentary xenoliths. The study of these samples has provided an unprecedented view of the source region of an island arc magmatic system with a propensity to produce giant porphyry-epithermal ore deposits. The xenolith assemblage includes spinel lherzolite, harzburgite, websterite, orthopyroxenite, clinopyroxenite, syenite, serpentinite, gabbro, hornblende gabbro, diabase, basalt, pelagic deep-sea sediment, and shallow-water volcaniclastic sediment as well as coralline and coralgal limestone. These lithologies represent a cross section of the suprasubduction assemblage and can be reassembled into an "ophiolite-type" model of oceanic lithosphere (Fig. 1) (*9*).

[1]Commonwealth Scientific and Industrial Research Organization Exploration and Mining, Post Office Box 136, North Ryde, New South Wales 1670, Australia; [2]Department of Earth Sciences, Monash University, Clayton, Victoria 3168, Australia; [3]Commonwealth Scientific and Industrial Research Organization Petroleum Resources, Post Office Box 136, North Ryde, New South Wales 1670, Australia.

*To whom correspondence should be addressed. E-mail: Brent.McInnes@dem.csiro.au

Most of the Tubaf ultramafic xenoliths are Cr-spinel harzburgites and were derived from depths ranging from 17 to 70 km (*10*). The harzburgites record a two-stage history of chemical depletion and enrichment (*11*): stage I, formation of a chemically depleted residue after the removal of 15 to 20% partial melt in a midocean ridge (MOR) environment; stage II, chemical enrichment associated with an oxidative, hydrous fluid metasomatism event.

Platinum group element (Pd, Pt, Ir, Ru, Rh, and Os), Au, Ni, Re, and Cu abundances were determined on six ultramafic rocks (five harzburgites and one orthopyroxenite) that exhibit a variety of styles and intensities of metasomatism (Table 1) (*12, 13*). The Ru, Rh, Ir, and Ni concentrations in metasomatized harzburgites are similar to those of an unmetasomatized harzburgite (sample 136063 in Table 1). These elements are therefore interpreted to be relatively insoluble in hydrous fluids. In contrast, enrichments of noble metals in the metasomatized ultramafic rocks are observed with Pd > Au > Pt > Re > Cu > Os and variations in abundance ranging from 2 to 800 times that of unmetasomatized harzburgite (Fig. 2). We interpret this order as an indication of the relative metal solubilities in hydrous fluids under mantle conditions (*14*). Replicate analyses of the orthopyroxenite vein (sample 136037) suggest that Os is heterogeneously distributed within the sample and is probably resident within the mackinawite (Fe-Ni sulfide) precipitate (*12, 15*). The alkalic arc basalt and cumulate xenoliths (phlogopite clinopyroxenite and syenite) have Re/Os ratios between 0.22 and 0.81, higher than those of the harzburgites (Re/Os < 0.1).

Previous studies (*9*) have demonstrated that the gabbro xenolith represents plutonic oceanic crust generated in a MOR environment during stage I partial melting. The Re content of 658 parts per trillion (ppt) and the Re/Os value of 990 for the gabbro fall within the range of MOR basalt values (*16*). The highly radiogenic Os isotopic composition of the gabbro (γOs = 1560) yields a model age for crust-mantle separation of 120 million years ago (Ma) (*17*) and indicates that the subarc basement of the New Ireland basin is Cretaceous oceanic crust (Fig. 1). The similarity in age of the subarc basement and the partially subducted Ontong Java Plateau (*18*) suggests that the Cretaceous Pacific Plate was subducting beneath its own detached fragment (Fig. 1).

The Os isotopic data for the ultramafic

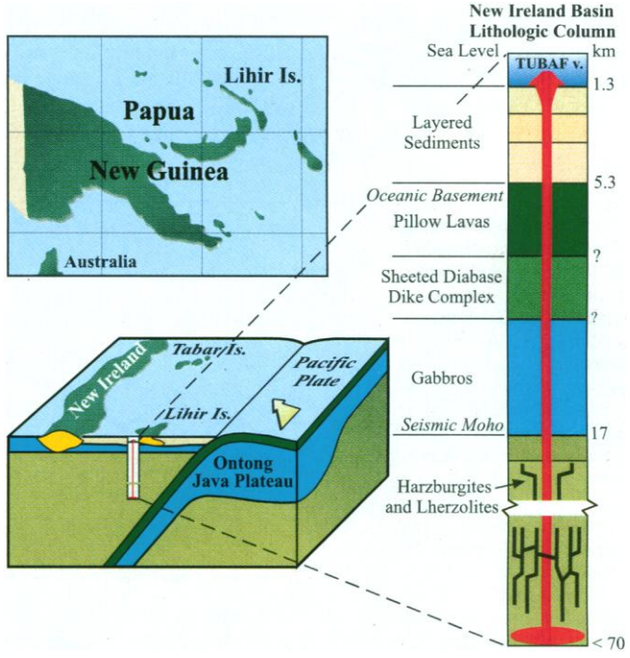

Fig. 1. Location map of the Tubaf volcano xenolith locality and petrological model of the New Ireland basin lithosphere constructed from seismic data (*10*) and by arranging xenolith assemblages according to their position in ophiolites (*9*). Westward subduction of the Pacific Plate into the Kilinailau trench since the Oligocene generated the New Ireland island arc, which shed 4 km of sediments into the New Ireland basin fore-arc depocenter. Collision of the Ontong Java Plateau with the trench about 10 Ma caused subduction to cease, and postcollisional alkaline arc volcanism (Tabar-Lihir-Tanga-Feni arc) in the New Ireland basin began about 3.5 Ma. A Re-Os crust-mantle separation age of 120 Ma for the New Ireland basin is similar to crustal ages for the Ontong Java Plateau (*18*) and indicates that Cretaceous Pacific Plate was subducting beneath its own detached fragment before the collision of the Ontong Java Plateau with the Kilinailau trench. Note that there is a break in scale for the mantle portion of the stratigraphic column.

Table 1. Bulk rock metal contents and Os-O isotopic systematics of rock samples from the Tubaf volcano xenolith locality and the Ladolam gold deposit from the Lihir Island group, Papua New Guinea. Noble metal contents are isotope dilution (Pd, Pt, Ir, Ru, Re, and Os) and external calibration (Rh, Au) ICP-MS analysis. Cu and Ni were determined by quantitative ICP-MS. All abundances are in ppb unless otherwise indicated. Dashes indicate no analysis. Geochemical data for primitive mantle are from (*33*). Oxygen isotope ratios are relative to SMOW. γOs is defined in (*17*).

Rock type	Sample	ppm										$^{187}Os/^{188}Os$ (2σ)		γOs (‰)	$\delta^{18}O$ (‰)
		Pd	Pt	Ir	Ru	Rh	Au	Cu	Ni	Os	Re				
Ultramafic rocks															
Harzburgite	136063	0.09	2.60	1.32	0.80	4.60	0.04	9	2428	3.1	0.009	0.12170	(27)	−4.3	4.9
Harzburgite	136061	1.30	18.80	<0.06	2.48	3.15	1.29	16	2254	6.3	0.029	0.13298	(27)	4.6	5.9
Harzburgite	136069	11.27	3.21	1.44	3.23	5.20	0.33	18	2446	2.2	0.075	0.13142	(51)	3.4	5.7
Harzburgite	136075	2.7	11.37	0.45	2.61	1.25	0.51	23	2248	3.8	0.032	0.13348	(29)	5	5.4
Harzburgite	136090	1.1	126.60	1.30	<.04	7.64	0.44	40	2654	—	—	—		—	5.4
Orthopyroxenite	136037	41.70	90.16	1.49	0.62	10.40	1.73	54	572	4.6	0.110	0.17851	(51)	40	6.5
Alkalic arc rocks															
Phlogopite clinopyroxenite	136036	—	—	—	—	—	—	—	—	0.52	0.116	0.14684	(52)	15.5	6.5
Basalt	136000	3.00	1.75	0.25	0.04	0.13	0.79	61	92	0.08	0.068	0.16723	(35)	31.6	6.5
Syenite	136031	21.30	15.50	7.91	0.47	3.39	0.13	145	183	0.22	0.082	0.14242	(46)	12.0	6.5
Oceanic crust															
Gabbro	136033	0.15	0.40	0.47	0.17	0.13	0.12	65	16	0.004	0.658	2.11696	(558)	1560	4.8
Gold ore samples															
Lihir ore	101201-1	—	—	—	—	—	—	—	—	0.16	10.27	0.14762	(45)	15.8	—
Lihir ore	101201-2	—	—	—	—	—	—	—	—	0.11	7.17	0.15176	(75)	19	—
Lihir ore	101373-1	—	—	—	—	—	—	—	—	0.02	94.01	0.52453	(1157)	311	—
Lihir ore	101373-3	—	—	—	—	—	—	—	—	0.07	9.56	0.21340	(320)	67	—

rocks (Table 1) (*19*) yield near-chondritic (*20*) values for types 1 and 2 [see (*12*)] harzburgites (γOs = −4.3 to +5.0), identical to those observed in samples from the Japan and Cascade arcs (γOs = −5 to +5) (*6*). The more radiogenic values for the type 3 orthopyroxenite vein assemblage (γOs = +40) requires a radiogenic slab-derived Os component. The host alkalic arc lava (shoshonite) and two cumulate xenoliths (syenite and phlogopite clinopyroxenite) also have relatively radiogenic Os values (γOs = +12 to +32). Data for Lihir ore sample 101373 (*21*) yielded an internal isochron producing a Re-Os age for gold mineralization of 690 ± 26 thousand years ago (Ka) (γOs = +62), consistent with K-Ar ages for the deposit (*22*). The narrow range in γOs (+32 to +62) for the orthopyroxenite vein, the alkalic arc lava, and the volcanic-hosted gold ores in Fig. 3 infers a common origin for the contained Os. However, the existence of subarc mantle veins with γOs greater than +40 (*7*) is suggested by the fact that the Lihir ores are more radiogenic than the orthopyroxenite vein.

To assess the degree of mass exchange between the slab and the mantle wedge, particularly the proportion of radiogenic Os derived from the slab, we analyzed oxygen isotopes (*23*). Oxygen isotope signatures in mantle rocks are a more robust measure of mass exchange between mantle and slab reservoirs during subduction, because, unlike other isotopic tracers (Sr, Nd), oxygen is an abundant constituent of each reservoir (*24*). Mantle xenoliths typically have a relatively narrow range in δ^{18}O [5.0 ± 0.5 per mil (‰)] (*25*), whereas subducted crustal material is enriched in ^{18}O during the process of low-temperature fluid-rock interaction (5.7 to 12‰) (*26*). Pressure- and temperature-induced dehydration of subducted crustal material will cause a flux of ^{18}O-enriched hydrous fluid to penetrate and interact with the overlying mantle wedge peridotite (*27*).

O-Os mixing models (*28*) indicate that the Lihir data can be reproduced by mixing 9% of a subduction component (95% oceanic crust and 5% oceanic sediment) with depleted mantle. A positive correlation between δ^{18}O and ^{187}Os/^{188}Os in the peridotite xenolith data (Fig. 3) suggests that there is a systematic variation between the type of metasomatism (fluid advection versus grain-boundary diffusion) and the amount of contamination of the slab component in the sample. The type 1 harzburgite is not metasomatized and has an isotopic composition similar to depleted mantle (*25*). In contrast, the orthopyroxenite vein sample (type 3) is enriched in ^{18}O and ^{187}Os, consistent with its formation by precipitation of metasomatic minerals from a subduction-derived fluid. A best-fit model curve linking the orthopyroxenite vein and the unmetasomatized harzburgite is obtained by using an $Os_{mantle}/Os_{slab\ fluid}$ mixing ratio of 11:1. The type 2 harzburgites have elevated δ^{18}O and γOs compared with depleted mantle, but the two-component models require $Os_{mantle}/Os_{slab\ fluid}$ mixing ratios around 30:1. These high ratios suggest that γOs and δ^{18}O are decoupled during diffusion of metasomatic fluids along grain boundaries. This may be due to the higher abundance of mantle Os contained within intergranular sulfides (*15*). Overall, the peridotite data imply that high γOs and δ^{18}O values are linked to metasomatic processes involving high fluid-to-mantle ratios.

The Os-O isotopic data for the plutonic (phlogopite clinopyroxenite and syenite) and volcanic (shoshonite lava host) samples form a linear array with a range in ^{187}Os/^{188}Os from 0.1424 to 0.1672 and with δ^{18}O values equivalent to the orthopyroxenite vein (~6.5‰) (Fig. 2). This data array may be explained by the generation of the plutonic and volcanic samples during partial melting of the metasomatized, veined mantle assemblages. These vein assemblages presumably have a lower solidus temperature than the unmetasomatized harzburgitic wall rock. The range in ^{187}Os/^{188}Os values may be caused by assimilation of mantle Os by the partial melt products in a mantle magma chamber. The variation in the γOs values between volcanic (+31) and plutonic (+12 to +15) rocks can be attributed to the residence time of the melt products in that chamber. The alkalic arc

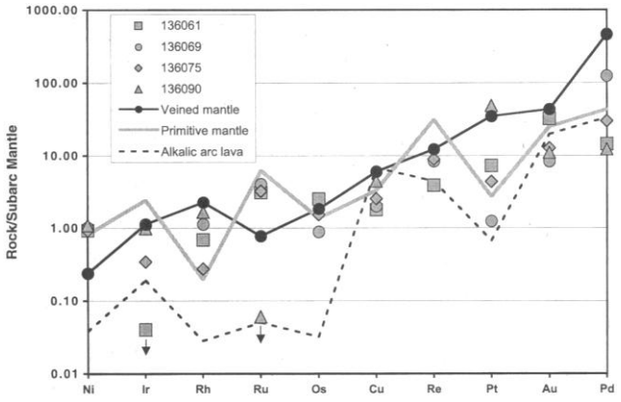

Fig. 2. Noble metal contents of veined mantle (sample 136037) and primitive mantle (*33*) relative to subarc mantle (fresh harzburgite sample 136063). Elements are arranged in order of increasing log-normalized average of the metasomatized Tubaf xenoliths. Samples with downward pointing arrows have abundances below the marked detection limits. Ni, Ir, and Rh are essentially insoluble in the hydrous fluids, whereas the solubility of the other metals increases from Os to Pd. Subduction-derived hydrous fluids have increased the Os, Cu, Pt, Au, and Pd values of metasomatized mantle to amounts that equal or exceed those of primitive mantle. Partial melting of these metasomatic veins produces metallogenically fertile alkalic arc lava enriched in Pd, Au, Re, and Cu.

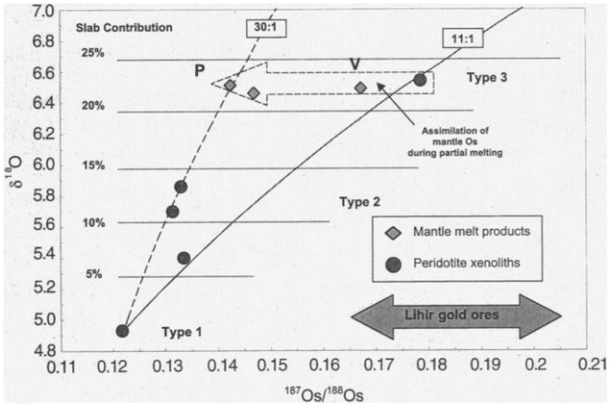

Fig. 3. Binary curves for the mixing of Os and O between end-member reservoirs consisting of depleted oceanic subarc mantle and subduction-derived fluids. The Os and O isotope composition of the depleted mantle end member is represented by the unmetasomatized harzburgite sample 136063 (δ^{18}O = 4.9‰ and ^{188}Os/^{187}Os = 0.1217), whereas the slab fluid end member is assumed to be derived from Cretaceous, seawater-altered oceanic crust of the Pacific Plate (δ^{18}O = 12‰ and ^{187}Os/^{188}Os = 2.117). Because isotopic fractionation is negligible at mantle temperatures, and the oxygen content of the mantle and slab fluid reservoirs are essentially the same (*24*), the contribution of slab-derived oxygen to the metasomatized peridotite varies from 8 to 13% for the type 2 (grain boundary diffusion-dominated) assemblage to 23% for the type 3 (advection-dominated) assemblage. The Lihir peridotite xenolith data can also be modeled with a series of $Os_{mantle}/Os_{slab\ fluid}$ ratios (curves of 30:1 and 11:1). Binary component mixing curves with an 11:1 ratio of $Os_{mantle}/Os_{slab\ fluid}$ best fit orthopyroxenite sample 136037, indicating that about 9% of the Os in the sample originated from a slab end member. The alkalic arc magmas [plutonic (P) and volcanic (V)] were generated by preferential partial melting of veined mantle assemblages. Whereas δ^{18}O remains unchanged during partial melting, the observed decrease in ^{187}Os/^{188}Os infers that up to 5% of type 1 mantle Os was assimilated before eruption. Gold ores from the volcano-hosted Ladolam mine have initial ^{187}Os/^{188}Os ratios that overlap values for the alkalic arc lava and its parental type 3 metasomatized mantle.

lava presumably had a relatively short mantle residence time because its γOs is nearly identical to the type 3 metasomatic vein (γOs = +40). If the syenite and phlogopite clinopyroxenite magmas had a longer residence time, there would be an increased potential for these magmas to dissolve low γOs sulfides in the harzburgite wall rock. Assimilation of <5% of mantle Os can drive a "vein melt" magma from +40 to values as low as +12 to +15 (*29*). Preferential partial melting of the veined mantle regions further fractionated the noble metals and produced an alkalic arc magma enriched in chalcophile elements (Au, Pd, Re, and Cu) (Fig. 2). Evidently Ni, Ir, Rh, Ru, Os, and Pt behave compatibly during the partial melting process, probably as a result of being partitioned into a magmatic sulfide phase.

Gold ores from the Ladolam deposit have Os isotope compositions similar to the subduction-modified mantle wedge peridotite that underlies it. The contribution of crustal Os to the mantle wedge is nominal (<10%), and we infer that the mantle is the primary source of ore metals in island arc settings. In a metallogenic context, the essential role of subduction is to produce a flux of oxidizing fluids capable of redistributing soluble metals within the mantle wedge under subsolidus conditions and concentrating them in sulfide-bearing metasomatic assemblages. Preferential partial melting of these assemblages favors the generation of arc magmas with elevated Au, Pd, and Cu contents. Because the subarc mantle is relatively depleted in Au, Cu, and Pd, processes that enhance the advective transport and concentration of fluid-soluble metals (Au, Cu, Pd, and Os) may be a prerequisite for generating of porphyry-epithermal Cu-Au deposits. We suggest that accretionary tectonic processes that lead to subduction cessation, such as occurred after the collision of the Ontong Java Plateau with the Kilinailau trench (Fig. 1), produce abnormally high fluid-to-mantle ratios because slab-derived fluids are effectively channeled through a vertical column of mantle wedge due to the shutdown of coupled slab subduction and mantle convection.

References and Notes

1. R. H. Sillitoe, *Econ. Geol.* **67**, 184 (1972); A. H. G. Mitchell and M. S. Garson, *Inst. Mining Metall. Trans.* **81**, B10 (1972); F. J. Sawkins, *J. Geol.* **80**, 377 (1972).
2. Pd, Pt, and Ru are commonly enriched in sulfide concentrates from porphyry deposits with the highest contents being recorded from gold-rich deposits, particularly those associated with alkaline porphyries [R. H. Sillitoe, in *Unconventional Metal Deposits*, W. C. Shanks, Ed. (American Institute of Mining, Metallurgy and Petroleum Engineering, New York, 1983), p. 207; F. E. Mutschler *et al.*, *Trans. Geol. Soc. S. Afr.* **88**, 355 (1985); D. Eliopoulos and M. Economou-Eliopoulos, *Econ. Geol.* **86**, 740 (1991); M. Tarkain and G. Koopman, *Mineral. Deposita* **30**, 39 (1995)]. Re and Os contents of base metal sulfides from the El Teniente porphyry Cu deposit in Chile range from 53 to 180 ppt and from 44 to 874 ppt, respectively [C. Freydier *et al.*, *Geology* **25**, 775 (1997)].
3. C. Ballhaus *et al.*, *Geochim. Cosmochim. Acta* **58**, 811 (1994); N. I. Bezmen *et al.*, *ibid.*, p. 1251 (1994); M. E. Fleet, J. H. Crocket, W. E. Stone, *ibid.* **60**, 2397 (1996); C. L. Peach, E. A. Mathez, R. R. Keays, *ibid.* **54**, 3379 (1990).
4. J. G. Foster *et al.*, *Nature* **382**, 703, (1996); D. D. Lambert *et al.*, *Econ. Geol.* **93**, 121 (1998); D. D. Lambert *et al.*, *J. Petrol.* **35**, 1717, (1994); T. E. McCandless and J. Ruiz, *Geology* **19**, 1225 (1991); R. J. Walker *et al.*, *Earth. Planet. Sci. Lett.* **105**, 416, (1991); R. J. Walker *et al.*, *Geochim. Cosmochim. Acta* **58**, 4179 (1994).
5. D. D. Lambert, J. G. Foster, L. R. Frick, D. M. Hoatson, A. C. Purvis, *Austr. J. Earth. Sci.* **45**, 265 (1998).
6. A. D. Brandon, R. A. Creaser, S. B. Shirey, R. W. Carlson, *Science* **272**, 861 (1996).
7. E. Widom and P. Kepezhinskas, *Eos Trans.* **80**, 354 (1999).
8. P. Herzig *et al.*, *ibid.* **75**, 513 (1994); P. M. Herzig and M. D. Hannington, in *PACRIM Congress 1995*, J. L. Mauk and J. D. St. George, Eds. (The Australasian Institute of Mining and Metallurgy, Auckland, New Zealand, 1995), vol. 9, pp. 279–284. Some of the samples used in this study were collected during Cruise SO-94 of RV *Sonne* (Edison project), which was organized by Freiberg University of Mining and Technology and funded by the German Federal Ministry for Research and Technology (BMFT grant 03G0094A to P. Herzig).
9. B. I. A. McInnes, P. M. Herzig, M. D. Hannington, R. A. Binns, *Eos* **75**, 747 (1994); B. I. A. McInnes, in *The Composition and Structure of Oceanic Lithosphere at a Convergent Plate Boundary*, R. Williams and H. Sloan, Eds. (ODP-InterRidge-IAVCEI, The Oceanic Lithosphere & Scientific Drilling into the 21st Century, Woods Hole, MA, 1996); B. I. A. McInnes, in *Research Review* (Commonwealth Scientific and Industrial Research Organization Exploration and Mining, North Ryde, New South Wales, Australia, 1999), vol. 1, pp. 11–13.
10. The sedimentary stratigraphy of the New Ireland Basin has been determined during geological and geophysical surveys [N. F. Exon *et al.*, *Bur. Miner. Resour. J. Austr. Geol. Geophys.* **10**, 39 (1986)]. The minimum depth estimate of 17 km for the ultramafic rocks is based on the depth of the Moho [A. S. Furomoto *et al.*, *Tectonophysics* **34**, 71 (1976)], and the maximum depth of 70 km is based on the absence of garnet-bearing peridotites.
11. B. I. A. McInnes, M. Gregoire, R. A. Binns, P. M. Herzig, M. D. Hannington, unpublished data; M. Gregoire, B. I. A. McInnes, S. O'Reilly, unpublished data.
12. The harzburgites can be subdivided into three textural types that span the spectrum from a depleted mantle end member to a fluid metasomatized end member: type 1, pristine anhydrous samples displaying ductile deformation; type 2, metasomatized samples with recrystallization of clinopyroxene and orthopyroxene grains, particularly along grain boundaries; type 3, metasomatized samples consisting of dilational veins containing metasomatic mineral precipitates. Type 3 veins are often observed to crosscut type 2 assemblages. The vein assemblage consists predominantly of peculiar fibrous, radiating orthopyroxene needles, and smaller amounts of clinopyroxene, olivine, Fe-Ni sulfides (approximating mackinawite in composition), phlogopite, and magnetite. Massive orthopyroxenite samples (up to 6 cm in diameter) presumably represent fragments of metasomatic vein material. The presence of H_2O-rich fluid inclusions in the orthopyroxene and the lack of shear structures in these veins indicates that metasomatism of peridotite occurred by hydraulic fracturing, probably as a result of the influx of slab-derived hydrous fluids into the mantle. The vein assemblage formed in equilibrium with an H_2O-rich supercritical fluid at 600° to 900°C and under high oxidation states [+1.5 to +3 log oxygen fugacity ($f O_2$) units above the fayalite-magnetite-quartz buffer (FMQ)] (*9, 11*).
13. The platinum-group elements (PGEs) were measured by isotope dilution (Pt, Pd, Ru, and Ir) and external calibration (Rh and Au) inductively coupled plasma mass spectrometry (ICP-MS). A mixed stable isotope spike (^{105}Pd, ^{198}Pt, ^{191}Ir, and ^{99}Ru) was added to 5 g of rock powder before digestion. Calibration standards were prepared for Au and Rh and were treated the same as samples. Ten reagent blanks (no spikes added) were also prepared and treated the same as samples in order to provide procedural blank values. Silicates were digested with hydrofluoric acid (HF) and PGEs were dissolved in aqua regia ($3HCl/HNO_3$). Samples with residue remaining after the treatment were fused in zirconium crucibles with a NaOH-Na_2O_2 flux, dissolved in HCl, and combined with the HF–aqua regia supernatant. Tellurium coprecipitation of PGE with stannous chloride (*30*) was used to separate analyte from matrix components. Filtered precipitate was dissolved in aqua regia and analyzed in 5 ml of 1.5 M nitric acid. Analysis of solutions on a Perkin Elmer Siex Elan model 5000 yielded detection limits of 0.1 part per billion (ppb) for Au and Pt, 0.01 to 0.05 ppb for Rh and Ru, and 0.006 ppb for Ir. These values were calculated as three times the standard deviation for the 10 reagent blanks. Precision for the technique as percent standard deviation for repeated analysis of Canadian Certified Reference Materials Project reference WGB-1 is 6% for Ir and Ru, 8% for Pt, 10% for Pd, 11% for Rh, and 14% for Au.
14. The solubility of PGEs and other metals in supercritical fluids at mantle conditions is largely unknown; although Au solubilities ranging from 30 to 1180 parts per million (ppm) (t = 550° to 725°C, P = 0.1 to 0.4 GPa) have been experimentally determined [R. R. Loucks and J. A. Mavrogenes, *Science* **284**, 2159 (1999)]. Pd solubilities up to 100 ppb in aqueous solutions (t = 500° to 800°C, P = 0.7 GPa, $f O_2$ = FMQ ± 1) have been calculated [D. C. Sassani and E. L. Shock, *Geology* **18**, 925 (1990)]. There are petrologic data for PGE enrichment under supercritical conditions in ophiolites [H. M. Prichard and M. Tarkian, *Can. Mineral.* **26**, 979 (1988)] and mafic intrusions [A. E. Boudreau, E. A. Mathez, I. S. McCallum, *J. Petrol.* **27**, 967 (1986)].
15. Isotopic analysis of 5 g of rock powder yielded higher Os and Re abundances (4.5 ppb Os and 0.11 ppb Re) and γOs values (+40) than duplicate 1-g analyses (0.55 ppb Os, 0.05 ppb Re, and γOs = +5 to +7). This suggests that the larger 5-g aliquot has sampled a heterogeneously distributed sulfide phase, which the smaller 1-g aliquots have missed (the nugget effect) (*30–32*). Mitchell and Keays (*31*) determined that the bulk (60 to 80%) of the PGEs and Au in the mantle are contained in sulfide-rich intergranular components in spinel lherzolite xenoliths. Hart and Ravizza (*32*) demonstrated that most Os in spinel lherzolite xenoliths from Kilbourne Hole was contained in sulfides (3.55 ppm Os), whereas olivine contained only 36 ppt Os.
16. P. Schiano, J.-L. Birck, C. J. Allegre, *Earth Planet. Sci. Lett.* **150**, 363 (1997); E. H. Hauri and S. R. Hart, *Chem. Geol.* **139**, 185 (1997).
17. Re-Os model age (T_{MA}) calculated as in ref. 25 of Hassler and Shimizu [D. R. Hassler and N. Shimizu, *Science* **280**, 418 (1998)] but with a decay constant for ^{187}Re of 1.666×10^{-11} [M. I. Smoliar, R. J. Walker, J. W. Morgan, *ibid.* **271**, 1099 (1996)], $(^{187}Os/^{188}Os)_{mantle}$ = 0.1271 [R. J. Walker *et al.*, *Geochim. Cosmochim. Acta* **58**, 4179 (1994)], and $(^{187}Re/^{188}Os)_{mantle}$ = 0.40076 [R. J. Walker and J. W. Morgan, *Science* **243**, 519 (1989)]. γOs is defined as the percentage difference between the sample and chondritic mantle at present day.
18. J. A. Tarduno *et al.*, *Nature* **254**, 399 (1991).
19. To avoid Re contamination from steel and tungsten carbide crushing equipment, we prepared all whole rock and mineral powders with a ceramic jaw crusher and agate mill. The jaw crusher and mill were thoroughly cleaned between samples by crushing multiple aliquots of clean quartz and precontaminating with an aliquot of the sample. We discarded the contaminated sample before we prepared a clean aliquot of rock powder. The Carius tube isotope dilution procedure used in the Monash laboratory to measure Re and Os concentrations and Os isotopic compositions is similar to that developed by Shirey and Walker [S. B. Shirey and R. J. Walker, *Anal. Chem.*

67, 235 (1995)], the details of which are described in (*5*). During this study, total chemistry and mass spectrometry blanks were 6 pg for Re and 2 pg for Os, with a $^{187}Os/^{188}Os$ blank ratio of 0.175. Blank corrections were insignificant for all samples analyzed in this study. Over a 3-year period, repeated analyses of an Os isotopic mass spectrometry standard provided by the Carnegie Institution of Washington, Department of Terrestrial Magnetism (DTM), made with Johnson-Matthey ammonium hexachlorosmate batch 5.56870-A, yielded mean $^{187}Os/^{188}Os = 0.17367 \pm 0.00058$ [external reproducibility at the 2σ level (n = 24) using a peak-jumping routine and a secondary electron multiplier], within error of the DTM value of 0.17429 ± 0.00055 [S. B. Shirey, *Can. J. Earth Sci.* **34**, 489 (1997)] (*5*). There is no measurable bias introduced into the data from our mass spectrometer (Finnigan MAT 262 N-TIMS) relative to results produced at DTM.

20. R. J. Walker, R. W. Carlson, S. B. Shirey, F. R. Boyd, *Geochim. Cosmochim. Acta*, **53**, 1583 (1989); M. Roy-Barman and C. J. Allegre, *ibid.* **58**, 5043 (1994); J. E. Snow and L. Reisberg, *Earth Planet. Sci. Lett.* **133**, 411 (1995).
21. The Lihir ore samples are from the Ladolam gold deposit and were selected from G. Carman's (1993) unpublished Ph.D thesis collection, Monash University. Sample 101373 is a biotite-altered basaltic breccia from the Minifie area containing the following alteration assemblage: biotite, potassium-containing feldspar (k-feldspar), anhydrite, calcite, pyrite, albite, quartz, adularia, chalcopyrite, tetrahedrite, electrum, galena, sphalerite, and argentite. Sample 101201 is a heterolithic breccia of mainly mafic lavas from the Lienetz area containing the following alteration assemblage: biotite, tourmaline, k-feldspar, albite, sericite, pyrite, magnetite, anhydrite, calcite, marcasite, and pyrrhotite.
22. K-Ar ages reported for various stages of hydrothermal alteration at the Ladolam gold deposit on Lihir island include the following: biotite separate from potassic altered volcanic rock age of 917 ± 100 Ka, biotite separate from biotite pyroxenite monzonite age of 343 ± 36 Ka, biotite separate from biotite-anhydrite vein age of 336 ± 27 Ka, and alunite-rich whole rock age of 151 ± 15 Ka [R. M. Davies and G. H. Ballantyne, in *PACRIM Congress 1987* (Australasian Institute of Mining and Metallargy, Gold Coast, Australia, 1987), vol. 1, pp. 943–994].
23. CO_2 for oxygen isotope analysis was prepared as described by Clayton and Mayeda [R. N. Clayton and T. K. Mayeda, *Geochim. Cosmochim. Acta* **27**, 43 (1963)]. Samples were finely ground and heated in Ni reaction vessels with BrF_5 at 650°C for 14 hours. The CO_2 was analyzed automatically on a Finnigan 252 mass spectrometer against an internal standard. Two quartz standards were run with every 10 samples. Replicate analysis of the standard quartz is generally better than ±0.2. Analyses are reported in per mil relative to the standard mean ocean water (SMOW) standard.
24. D. E. James, *Annu. Rev. Earth. Planet. Sci.* **9**, 311 (1981).
25. T. K. Kyser, in *Stable Isotopes in High Temperature Geological Processes*, J. W. Valley, H. P. Taylor Jr., J. R. O'Neill, Eds. (Mineralogical Society of America, Washington, DC, 1986), vol. 16, pp. 141–164.
26. J. D. Cocker, T. J. Griffin, K. Muehlenbachs, *Earth Planet. Sci. Lett.* **61**, 112 (1982); R. T. Gregory and H. P. Taylor Jr., *J. Geophys. Res.* **86**, 2737 (1981); K. Muehlenbachs, in *Stable Isotopes in High Temperature Geological Processes*, J. W. Valley, H. P. Taylor Jr., J. R. O'Neill, Eds. (Mineralogical Society of America, Washington, DC, 1986), vol. 16, pp. 425–444.
27. Melt inclusions from mantle wedge samples from the Tabar-Lihir-Tanga-Feni island arc are enriched in ^{18}O, with $\delta^{18}O$ values ranging from 9.0 to 11.3‰ ± 1.1‰; J. M. Eiler, B. I. A. McInnes, J. W. Valley, C. M. Graham, E. M. Stolper, *Nature* **393**, 777 (1998).
28. The calculations follow the method outlined in (*6*). The Os abundances in the oceanic basalt and oceanic sediment were assumed to be equal. The Os isotopic composition of the subduction component was calculated with the following parameters: oceanic sediment $^{187}Os/^{188}Os = 1.023$ [an average value based on references in (*6*)] and oceanic basalt $^{187}Os/^{188}Os = 2.117$ (assumes slab basalt has $^{187}Os/^{188}Os$ equivalent to gabbro sample 136033 in Table 1). Therefore, a 95% slab basalt containing 5% oceanic sediment slab component will have $^{187}Os/^{188}Os = 2.062$. The depleted peridotite end-member component was assumed to have an isotopic composition equivalent to harzburgite sample 136063 in Table 1 ($^{187}Os/^{188}Os = 0.1217$ and $\delta^{18}O = 4.9‰$). The $\delta^{18}O$ for the subduction component is ascribed a value of 12‰ based on $\delta^{18}O$ measurements of subduction-derived metasomatic agents with $\delta^{18}O = 11.3‰$ from mantle wedge xenocrysts found elsewhere in the Tabar-Lihir-Tanga-Feni arc (*27*). The value of 12‰ is consistent with values obtained from seawater-altered basalt (5.7 to 12‰) from the upper 1 to 2 km of oceanic crust from ophiolite sequences (*26*).
29. Modeling assumes simple bulk mixing between Lihir melt ($^{187}Os/^{188}Os = 0.167$, Os = 0.080 ppb; sample 136000 in Table 1) and peridotite mantle [$^{187}Os/^{188}Os = 0.122$ to 0.1271, Os = 3.5 ppb; see Table 1 and (*18*)].
30. S. B. Shirey and R. W. Walker, *Anal. Chem.* **67**, 2136 (1995)
31. R. H. Mitchell and R. R. Keays, *Geochim. Cosmochim. Acta* **45**, 2425 (1981).
32. S. R. Hart and G. Ravizza, *Eos* 120 (1993).
33. W. F. McDonough and S.-s. Sun, *Chem. Geol.* **120**, 223 (1995).
34. We thank John Byrne and Jim Keegan for assistance in determining PGE contents, Brad McDonald for oxygen isotope analysis, and Eva Mylka for drafting. The comments of the anonymous reviewers helped clarify the presentation.

22 June 1999; accepted 3 September 1999

Continuous Deformation Versus Faulting Through the Continental Lithosphere of New Zealand

Peter Molnar,[1]* Helen J. Anderson,[2,3,4] Etienne Audoine,[5] Donna Eberhart-Phillips,[3] Ken R. Gledhill,[6] Eryn R. Klosko,[7,8] Thomas V. McEvilly,[9] David Okaya,[10] Martha Kane Savage,[5] Tim Stern,[5] Francis T. Wu[7]

Seismic anisotropy and *P*-wave delays in New Zealand imply widespread deformation in the underlying mantle, not slip on a narrow fault zone, which is characteristic of plate boundaries in oceanic regions. Large magnitudes of shear-wave splitting and orientations of fast polarization parallel to the Alpine fault show that pervasive simple shear of the mantle lithosphere has accommodated the cumulative strike-slip plate motion. Variations in *P*-wave residuals across the Southern Alps rule out underthrusting of one slab of mantle lithosphere beneath another but permit continuous deformation of lithosphere shortened by about 100 kilometers since 6 to 7 million years ago.

In most oceanic regions, plates of lithosphere move past one another along narrow boundaries (width <20 km), and a single major fault can define transform and convergent boundaries; active deformation within continental regions, however, commonly spans dimensions of hundreds to thousands of kilometers. The much greater creep strength of olivine than of crustal minerals makes oceanic lithosphere strong in the depth range where continental lithosphere appears to be weakest (*1*). What then is the role of the mantle lithosphere beneath continents? Is it cut by faults, or narrow shear zones, that separate effectively rigid bodies, as if plate tectonics occurred but was blurred by the easily deformed overlying crust (*2*, *3*); or does the mantle lithosphere deform continuously over a wide area, behaving as a continuous medium (*4*, *5*) (Fig. 1)? New Zealand offers tests of these possibilities. Since ~45 million years ago (Ma), the Pacific and Australian plates have slid 850 (±100) km past one another, with ~460 km of right-lateral slip on a single major fault, the Alpine fault, dominating Cenozoic deformation of New Zealand's crust (*6*, *7*). Does the Alpine fault cut through the entire lithosphere, or does widespread simple shear

[1]Quaternary Research Center and Geophysics Program, University of Washington, Seattle, WA, 98195-1360, USA, and Department of Earth Atmospheric and Planetary Sciences, Massachusetts Institute of Technology, Cambridge, Massachusetts 02139, USA. [2]Ministry of Research, Science and Technology, Post Office Box 5336, Wellington, New Zealand. [3]Institute of Geological and Nuclear Sciences, Private Bag 1930, Dunedin, New Zealand. [4]Otago University, Dunedin, New Zealand. [5]Institute of Geophysics, School of Earth Sciences, Victoria University of Wellington, Wellington, New Zealand. [6]Institute of Geological and Nuclear Sciences, Gracefield Research Centre, Post Office Box 30–368 Lower Hutt, Wellington, New Zealand. [7]Department of Geological Sciences, State University of New York, Binghamton, NY, 13902, USA. [8]Department of Geological Sciences, 1847 Sheridan Road, Locy Hall, Northwestern University, Evanston, IL 60208, USA. [9]Berkeley Seismological Laboratory, University of California, Berkeley, CA 94720, USA. [10]Department of Earth Sciences, University of Southern California, Los Angeles, CA 90089, USA.

*To whom correspondence should be addressed. E-mail: molnar@chandler.mit.edu

References and Notes

[6] **Osmium Recycling in Subduction Zones**
Alan D. Brandon; Robert A. Creaser; Steven B. Shirey; Richard W. Carlson
Science, New Series, Vol. 272, No. 5263. (May 10, 1996), pp. 861-864.
Stable URL:
http://links.jstor.org/sici?sici=0036-8075%2819960510%293%3A272%3A5263%3C861%3AORISZ%3E2.0.CO%3B2-3

[14] **Gold Solubility in Supercritical Hydrothermal Brines Measured in Synthetic Fluid Inclusions**
Robert R. Loucks; John A. Mavrogenes
Science, New Series, Vol. 284, No. 5423. (Jun. 25, 1999), pp. 2159-2163.
Stable URL:
http://links.jstor.org/sici?sici=0036-8075%2819990625%293%3A284%3A5423%3C2159%3AGSISHB%3E2.0.CO%3B2-M

[17] **Osmium Isotopic Evidence for Ancient Subcontinental Lithospheric Mantle Beneath the Kerguelen Islands, Southern Indian Ocean**
Deborah R. Hassler; Nobumichi Shimizu
Science, New Series, Vol. 280, No. 5362. (Apr. 17, 1998), pp. 418-421.
Stable URL:
http://links.jstor.org/sici?sici=0036-8075%2819980417%293%3A280%3A5362%3C418%3AOIEFAS%3E2.0.CO%3B2-%23

[17] **Rhenium-Osmium Isotope Systematics of Carbonaceous Chondrites**
R. J. Walker; J. W. Morgan
Science, New Series, Vol. 243, No. 4890. (Jan. 27, 1989), pp. 519-522.
Stable URL:
http://links.jstor.org/sici?sici=0036-8075%2819890127%293%3A243%3A4890%3C519%3ARISOCC%3E2.0.CO%3B2-S